JACS
JOURNAL OF THE AMERICAN CHEMICAL SOCIETY

ARTICLE

pubs.acs.org/JACS

Mapping the Reaction Coordinates of Enzymatic Defluorination

Peter W. Y. Chan,[†,⊥] Alexander F. Yakunin,[‡] Elizabeth A. Edwards,[§] and Emil F. Pai*[,†,⊥,∥]

[†]Department of Biochemistry, [‡]Structural Proteomics in Toronto, Banting and Best Department of Medical Research, [§]Department of Chemical Engineering and Applied Chemistry, and [∥]Departments of Medical Biophysics and Molecular Genetics, University of Toronto, Toronto, Ontario M5S 1A8, Canada

[⊥]Ontario Cancer Institute/The Campbell Family Cancer Research Institute, University Health Network, Toronto, Ontario M5G 2C4, Canada

Supporting Information

ABSTRACT: The carbon−fluorine bond is the strongest covalent bond in organic chemistry, yet fluoroacetate dehalogenases can readily hydrolyze this bond under mild physiological conditions. Elucidating the molecular basis of this rare biocatalytic activity will provide the fundamental chemical insights into how this formidable feat is achieved. Here, we present a series of high-resolution (1.15−1.80 Å) crystal structures of a fluoroacetate dehalogenase, capturing snapshots along the defluorination reaction: the free enzyme, enzyme−fluoroacetate Michaelis complex, glycolyl−enzyme covalent intermediate, and enzyme−product complex. We demonstrate that enzymatic defluorination requires a halide pocket that not only supplies three hydrogen bonds to stabilize the fluoride ion but also is finely tailored for the smaller fluorine halogen atom to establish selectivity toward fluorinated substrates. We have further uncovered dynamics near the active site which may play pivotal roles in enzymatic defluorination. These findings may ultimately lead to the development of novel defluorinases that will enable the biotransformation of more complex fluorinated organic compounds, which in turn will assist the synthesis, detoxification, biodegradation, disposal, recycling, and regulatory strategies for the growing markets of organofluorines across major industrial sectors.

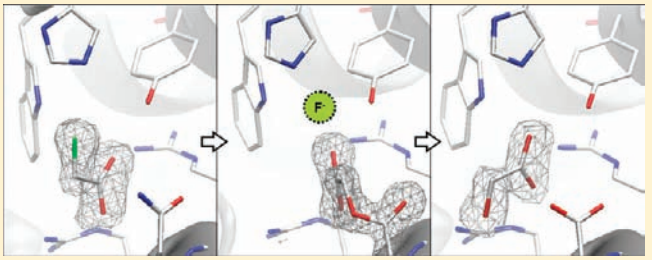

INTRODUCTION

Fluorine forms the strongest single bond to carbon, with a dissociation energy of up to 130 kcal/mol, the highest among all natural products.[1,2] This unrivaled stability arises because fluorine is the most electronegative element, which introduces reinforcing ionic forces through strong polarization of this bond. The reactivity of the C−F bond is further lowered due to the poor accessibility to the valence electrons of the bonded fluorine atom.[3,4]

Fluorinated organic compounds are renowned for their unique features including inertness, hydrophobicity, and even lipophobicity.[5,6] Owing to these physicochemical properties, organofluorines are widely and increasingly used in numerous industries.[1,2,6,7] For example, fluorinated compounds presently compose 20% of all pharmaceuticals and up to 30% of all agrochemicals.[8] However, the large-scale production and application of anthropogenic organofluorines have increasingly become subjects of debate due to the toxicity, global warming potential, ozone depletion, environmental persistence, and bioaccumulation of the compounds.[4,9−11] A deeper understanding of the molecular mechanisms underlying the cleavage of the highly stable C−F bond is therefore of growing importance for the development of efficient strategies for degrading fluorinated organic compounds.[4]

Several microbial enzymes that break the C−F bond have been described.[12,13] Among the first ones was the fluoroacetate dehalogenase (FAcD) discovered in a pseudomonad in 1965.[1] It hydrolyzes various short-chain 2-haloacids with fluoroacetate (FAc) as its preferred substrate.[14−17] FAc is very stable, with an estimated half-life of over 47 years in water.[18] It is the most common among the rare natural organofluorine compounds, synthesized by the thienamycin-producing actinobacterium *Streptomyces cattleya* as a secondary metabolite and by numerous plants as a defense against grazing.[19,20] To mammals, FAc is one of the most toxic poisons because of its close resemblance to acetate; it is transformed by "lethal synthesis" *in vivo* into fluorocitrate, the source of a highly potent inhibitor blocking both the aconitase of the citric acid cycle and the citrate transport machinery across the mitochondrial membrane.[19−21] For this purpose, FAc also serves as a commercial rodenticide, codenamed "Compound 1080", in Australia, Israel, Mexico, New Zealand, and the United States.[22]

Despite the potential environmental and industrial applications of defluorinases, their mode of action has not been extensively characterized. In FAcDs, defluorination was proposed to involve

Received: January 11, 2011
Published: April 21, 2011

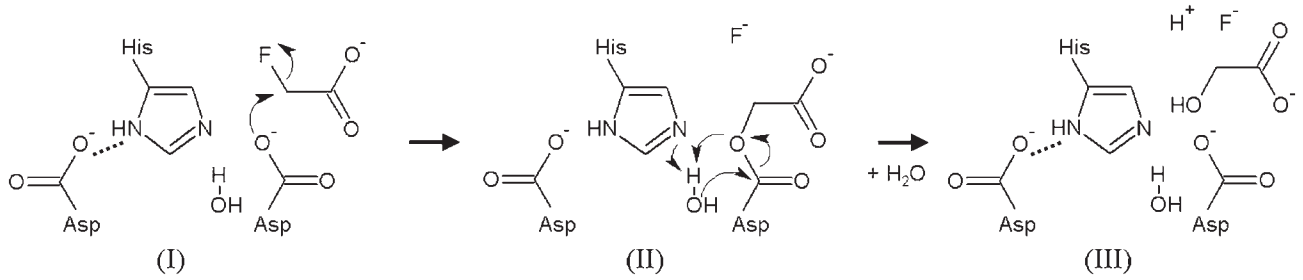

Figure 1. Proposed two-step reaction mechanism of fluoroacetate dehalogenases. Catalysis involves the conserved aspartate−histidine−aspartate catalytic triad.[15] The reaction cycles from the free enzyme, Michaelis complex (I), covalent ester intermediate (II), enzyme−product complex (III), and then back to the free enzyme. First, fluoride is displaced by the aspartate nucleophile in an S_N2 attack. The resulting covalent intermediate is then hydrolyzed by a water molecule activated by the histidine base. This step is assisted by the second aspartate residue.

Table 1. Summary of Crystal Structures of RPA1163 and Mutants[a]

	catalytic event					
	free enzyme	Michaelis complex			covalent intermediate	product complex
enzyme/ligand	WT/apo	D110N/FAc	D110N/ClAc	D110N/BrAc	H280N/FAc	WT/GOA
PDB code	3R3U	3R3V	3R3W	3R3X	3R3Y	3R3Z
resolution (Å)	1.60	1.50	1.60	1.80	1.15	1.70
R/R_{free} (%)	17.2/20.2	18.6/22.3	18.1/22.3	19.2/23.3	15.3/18.7	17.9/21.8

[a] The structures of the complexes were produced by soaking experiments. FAc, ClAc, BrAc, and GOA denote fluoroacetate, chloroacetate, bromoacetate, and glycolate, respectively.

an S_N2 attack in which an aspartate nucleophile directly ejects the fluoride anion from the substrate (Figure 1).[15,17] Although this mechanism parallels that of the structurally homologous, but non-defluorinating, haloalkane dehalogenases as well as the L-2-haloacid dehalogenases,[15,23−26] the structural features that specifically confer defluorinating activity remain unclear. The crystal structure of the FAcD from *Burkholderia* sp. FA1 identified the active site containing the aspartate nucleophile. The nearby histidine and tryptophan residues were proposed to stabilize the leaving fluoride on the basis of their binding to chloride.[27] Subsequent theoretical studies predicted that an additional tyrosine residue participates in fluoride stabilization to assist the cleavage of the C−F bond.[28] Interestingly, although the C−F bond is recognized as one of the strongest covalent bonds, activating this bond by employing acetate as nucleophile in an S_N2 mechanism may require only ∼20 kcal/mol.[28] Given this relatively low activation energy, it is puzzling as to why most dehalogenating enzymes exhibit no defluorination activity. Illuminating the unique structural requirements which enable defluorination should be a first step toward the development of enzymes, possibly with the help of powerful emerging techniques such as *de novo* computational design,[29] which eventually will be able to degrade even the notoriously persistent perfluorocarbons.

To explore the molecular basis of enzymatic defluorination and the preferential hydrolysis of the C−F bond over weaker carbon−halogen bonds by FAcDs, we have structurally and biochemically characterized the FAcD RPA1163. This defluorinase was discovered in a functional genomic screen of the photosynthetic bacterium *Rhodopseudomonas palustris* CGA009,[30] which is well known for its metabolic versatility and bioremediation potential. Our high-resolution crystal structures reveal for the first time the structures of intermediates for each step of the defluorination reaction (Table 1).

RESULTS AND DISCUSSION

Overall Structure of RPA1163. The apo-structure of WT RPA1163 shows a homodimeric protein with an α/β hydrolase fold,[23] comprising an $\alpha/\beta/\alpha$ core linked to an α-helical cap (Figure 2). The conserved catalytic triad (Asp110 nucleophile, His280 base, and Asp134 carboxylate) marks the active site location, which is buried in the domain interface and accessible only via an 11-Å-long channel (Figure 2).

When compared to the *Burkholderia* FAcD (42% sequence identity; Supporting Information, Figure S1), the overall folds of the two enzymes are highly similar, with a root-mean-square deviation (rmsd) of 1.1 Å for all Cα atoms (Figure 3A). Both FAcDs share an active site identical in composition, which also comprises Phe40, Arg111, Arg114, His155, Trp156, Trp185, and Tyr219 (RPA1163 numbering). Moreover, the spatial arrangement of these residues is strikingly well conserved: a least-squares fit of the 77 non-hydrogen atoms from seven of these residues (Asp110, Arg111, Arg114, His155, Trp156, Tyr219, and Phe40) yields an rmsd of only 0.19 Å (Figure 3C). This suggests that defluorination requires a highly precise arrangement of active site residues and bonding geometries.

The largest conformational difference between RPA1163 and the *Burkholderia* FAcD is found in a loop of the α-helical cap domain (Figure 3A). This loop harbors Trp185 (RPA1163 numbering), which is in close proximity to the fluoride pocket (discussed below). In RPA1163, this loop makes several contacts with the $\alpha/\beta/\alpha$ core domain. In the *Burkholderia* FAcD, however, it is lifted outward and becomes more exposed to solvent. As a result, the corresponding tryptophan side chain in the *Burkholderia* FAcD is driven ∼8 Å farther away from the fluoride pocket (Figure 3B). This cap domain loop in FAcD may therefore exhibit significant mobility.

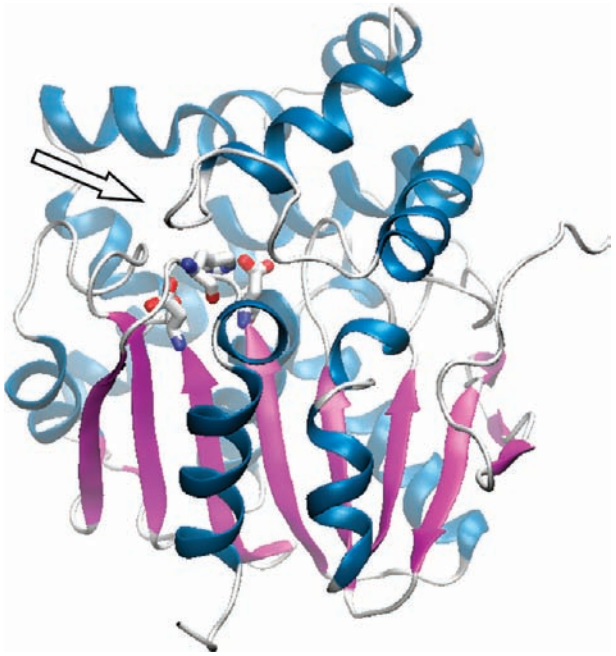

Figure 2. Overall structure of RPA1163. The upper and lower domains are the α-helical cap and α/β/α core, respectively. The catalytic triad Asp110-His280-Asp134 protruding from the core domain is shown as sticks. The arrow indicates the opening of the 11-Å-long channel leading to the active site.

Structure of the Enzyme−Substrate Complex. The binding of substrate is illustrated by the Michaelis complex in which the intact FAc molecule is trapped in the active site of the catalytically inactive nucleophile mutant Asp110Asn (Figure 4B). The carboxylate oxygen atoms of FAc are coordinated to Arg111 (O1−Nη1 2.7 Å) and Arg114 (O2−Nε 2.8 Å and O2−Nη1 3.0 Å), and through a hydrogen bond to Tyr219 (O1−Oη 2.8 Å). The fluorine atom is bound by His155 (F−Nε2 3.0 Å), Trp156 (F−Nε1 3.3 Å), and Tyr219 (F−Oη 3.2 Å), suggesting their contributions to weakening the C−F bond and stabilizing the displaced fluoride ion. Further destabilization of the C−F bond is likely accomplished by placing the fluorine-bearing carbon atom (C2) of FAc close (∼3 Å) to Oδ2 of the Asp110 nucleophile in WT RPA1163, which has been substituted by Nδ2 in this mutant. The C−F bond forms a 99° angle with C2--Nδ2 (or 105° with C2--Oδ2 when superposing the FAc molecule onto the WT structure), which is far from the anticipated 180° angle. The altered shape and electrostatics of the active site have apparently kept C2 of FAc slightly (∼1.4 Å, see next section) out of its near-attack conformation. Nevertheless, given the largely unmodified bonding network in the active site and the highly similar ligand binding modes among the structures of the various reaction intermediates, this enzyme−substrate complex probably closely represents the active site organization prior to the S_N2 nucleophilic attack.

Cleavage of the C−F Bond by Nucleophilic Attack. The S_N2 reaction is initiated by the Oδ2 atom of Asp110 attacking C2 of FAc to expel the fluoride, with inversion of stereochemistry at C2. The cleavage of the C−F bond results in the simultaneous formation of the glycolyl−enzyme covalent intermediate (Figure 1). This structure is captured using the His280Asn mutant which no longer has the histidine base to activate the catalytic water required for hydrolyzing the covalent intermediate (Figure 4C). Compared with the Michaelis complex, the C2 of the substrate moiety (formerly FAc) is shifted 1.4 Å deeper into the active site to covalently link to Oδ2 of Asp110 (Figure 4E). This newly formed O−C bond points directly toward a cavity lined by His155, Trp156, and Tyr219. With S_N2 reactions imposing a collinear alignment from the nucleophile (Oδ2), electrophile (C2), to the leaving atom (fluoride), this geometric arrangement further implicates the role of these three aromatic residues in stabilizing the fluoride ion (Figure 4E,F). Soaking of His280Asn/FAc crystals in as much as 0.1 M NH_4F produced no additional electron density inside the fluoride pocket. This low affinity for free fluoride suggests that the displaced fluoride is irreversibly shuttled to the bulk solvent. This process may be assisted by the highly dynamic Trp185 in the proximity of the fluoride pocket (discussed below), possibly through a "flapping" motion (Figure 4F).

It is worth noting that the line of the S_N2 attack (i.e., F--C2--Oδ2) appears nearly coplanar with FAc's carboxylate group. This is distinct from the anticipated orthogonal orientation in free solution, which according to *ab initio* calculations allows FAc's carboxylate group to assist transition-state stabilization by delocalizing its π-electrons into the adjacent orbitals of the breaking C−F and forming C−O bonds.[31] Although it is not clear why FAcDs do not harness the stabilization energy intrinsic to this attack conformation, one could argue that the molecular evolution of FAcDs has yet to be perfected. The strongest evolutionary pressure for further acceleration of C−F bond cleavage, however, may have well been removed, considering that this step is not rate-limiting in FAc hydrolysis[28] and that the current catalytic rates are already sufficient to ensure the survival of the host organism.

Hydrolysis of the Covalent Intermediate. Subsequently, the glycolyl-Asp110 ester intermediate is hydrolyzed to complete the catalytic cycle. As shown in the WT/glycolate product complex (Figure 4D,G), this involves an attack on Cγ of Asp110 by the nearby water molecule present in most structures (Cγ−O 3.1 ± 0.1 Å) (Figure 4D). This is likely facilitated by the simultaneous abstraction of a proton from the catalytic water by the His280 base (O−Nε2 3.1 Å), assisted in turn by Asp134 (Nδ1−Oδ1 2.6 Å). Hydrolysis of the ester intermediate is also expected to proceed via a tetrahedral intermediate, in which the transient negative charge on Oδ1 of Asp110 is stabilized by an oxyanion hole formed by the backbone amides of Phe40 (Oδ1−N 2.8 Å) and Arg111 (Oδ1−N 2.8 Å).

In the WT/glycolate product complex, the carboxylate group of glycolate is coordinated to Arg111 and Arg114, resembling the substrate in the Michaelis complex (Figure 4B,D). Interestingly, one of the carboxylate oxygen atoms is hydrogen-bonded to the halide pocket residues His155, Trp156, and Tyr219. The hydroxyl group of glycolate is located close (3.4 Å) to Oδ2 of Asp110 (Figure 4G). Since this hydroxyl group is derived from Oδ2 of Asp110, this complex probably reveals the initial departure of glycolate before it completely dissociates from the enzyme.

Structural Basis for Halide Selectivity and Enzymatic Defluorination. RPA1163 displays a remarkable preference for FAc hydrolysis over that of ClAc or BrAc, despite FAc containing the stronger carbon−halogen bond (Table 2 and Supporting Information, Figure S8). This trend appears to correlate with the increase in size of the halide atom (van der Waals radii: F = 1.47 Å, Cl = 1.75 Å, and Br = 1.85 Å). To rationalize the structural basis of the selectivity for FAc, the Michaelis complex structures with ClAc and BrAc were also determined (Table 1 and

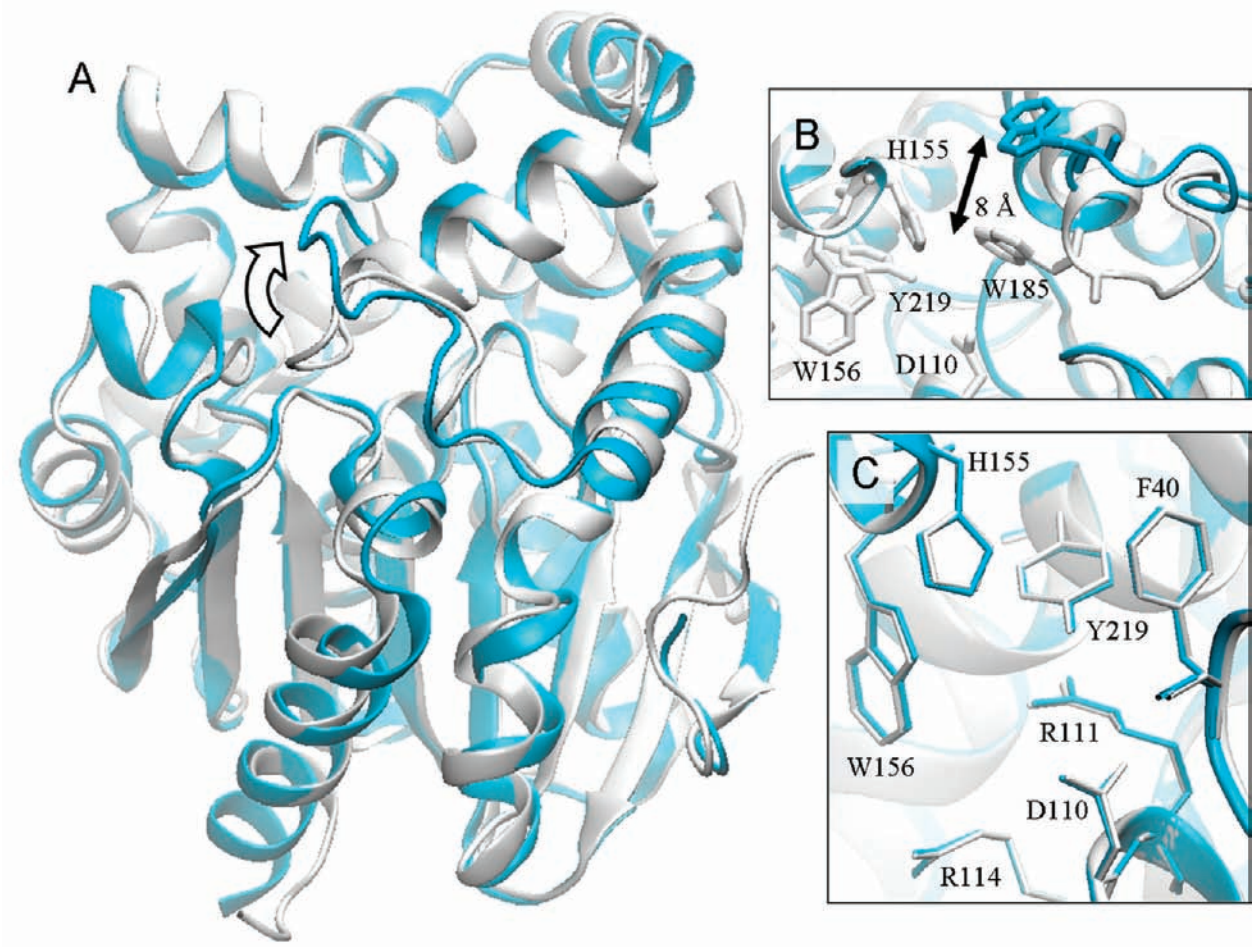

Figure 3. Structural comparison between RPA1163 and the *Burkholderia* FAcD. The secondary structural elements of RPA1163 (gray) superpose well onto those of the *Burkholderia* FAcD (cyan). (A) At the active site entrance, the cap domain loop which carries Trp185 displays the largest conformational difference (curved arrow). (B) The active site cavity viewed along the access tunnel. The corresponding tryptophan side chain in the *Burkholderia* FAcD is located ~8 Å farther away from the active site. (C) Superposition of seven catalytically important residues reveals a remarkably conserved active site architecture.

Figure 5A). The comparison of the RPA1163 active sites in the three complexes suggests that only His155 has the elasticity to yield additional space in the halide pocket. Compared to the Asp110Asn/FAc complex, the imidazole ring of His155 is retracted 0.30 and 0.36 Å from the halide cavity in the ClAc and BrAc complexes, respectively (Figure 5B). However, the motional freedom of His155 alone seems insufficient for allowing the FAcD to readily accommodate larger haloacetates since the larger halogen atoms are kept farther out of the halide pocket, apparently withholding the substrate from binding deeper within the active site (Figure 5B). Therefore, the lower activity of FAcD toward larger haloacetates (despite their weaker C−X bonds) is likely caused by the increased energy barrier required to overcome the steric hindrance from "squeezing" the larger halide into too small a pocket in order to achieve acceptable reaction geometry.

Steady-state kinetics measurements for FAc hydrolysis by RPA1163 mutants reveal that His155Asn, Trp156His, and Tyr219Phe all have a significantly reduced k_{cat} but a generally unaffected K_m (Table 2). This is consistent with the proposed role of these residues in fluoride stabilization. Mutations to the nearby Phe40 and "flapping" Trp185 also disrupt dehalogenation activity, but the precise functions of these two amino acids are still speculative.

RPA1163 displays 5-fold higher activity (k_{cat}) toward FAc than toward ClAc (Table 2). Intriguingly, this substrate preference can be reversed by the His155Asn and Tyr219Phe mutations. In His155Asn, the mutation enlarges the halide pocket to relieve steric constraints without disrupting the electrostatic environment. This enhances ClAc turnover 4-fold compared to WT, which contributes significantly to the 8-fold higher activity on ClAc than FAc. In Tyr219Phe, deleting the hydroxyl group enlarges the halide pocket at the cost of a polar contact, thereby removing both steric constraints and electrostatic stabilization. Although this slows both defluorination and dechlorination activities, it is the much larger 190-fold drop in FAc turnover that accounts for the 12-fold higher ClAc activity over FAc. These results suggest that steric effects dictate the halide selectivity, whereas electrostatic stabilization determines the overall catalytic efficiency of the enzyme.

Dynamics of RPA1163. The initial comparison between RPA1163 and the *Burkholderia* FAcD suggests the possibility of large conformational freedom of the active site loop which bears Trp185 (Figure 3A,B, discussed above). This is consistent with the elevated *B*-factors and the survey of all Trp185 conformations in 20 RPA1163 structures (including additional reference structures presented in the Supporting Information),

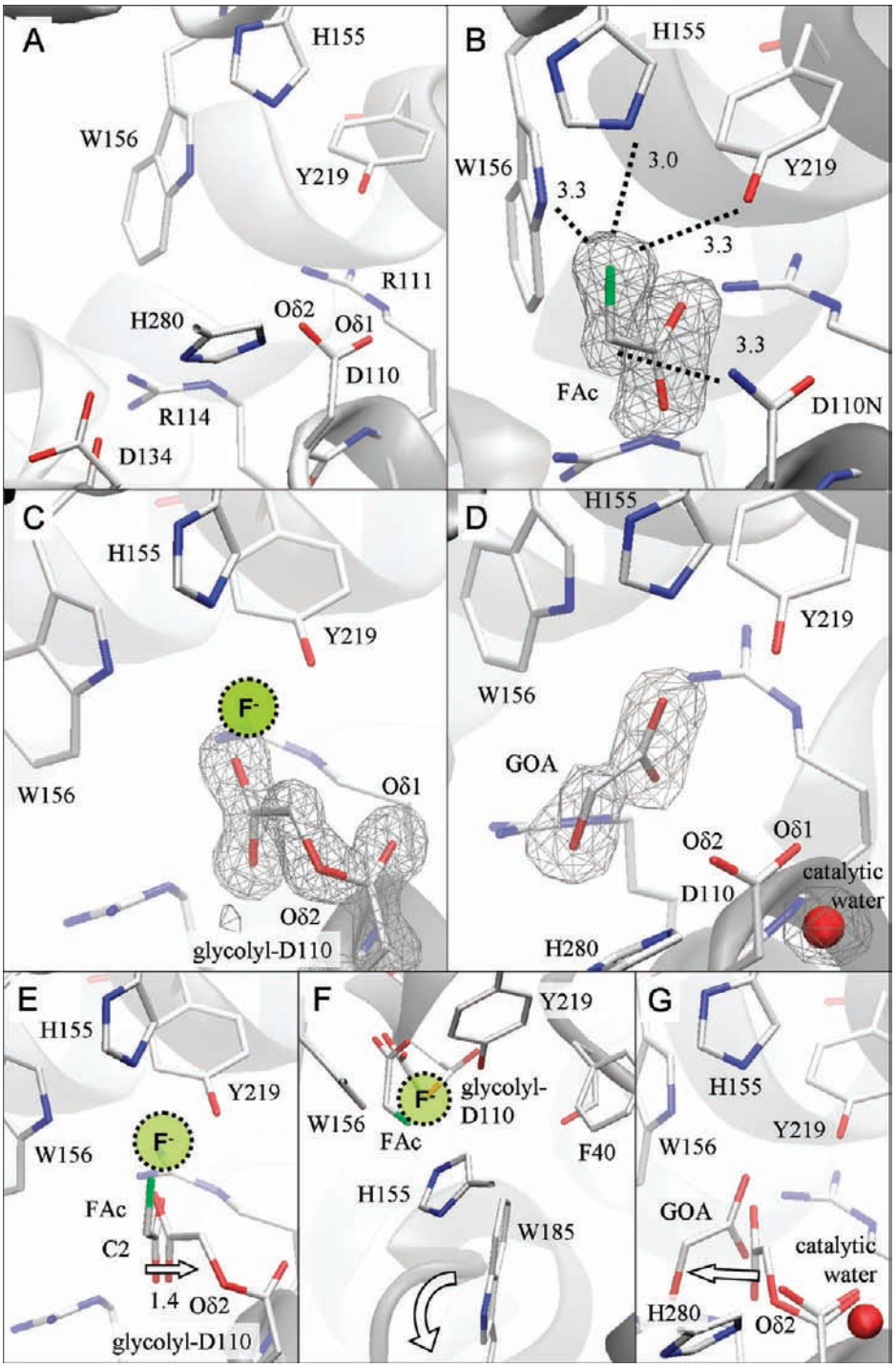

Figure 4. Structural comparison of reaction intermediates reveals the progress of enzymatic defluorination in RPA1163. (A) Active site structure of the free WT FAcD. The cavity comprises the catalytic triad (Asp110-His280-Asp134), the carboxylate binding site (Arg111 and Arg114), and the fluoride pocket (His155, Trp156, and Tyr219). (B) The Asp110Asn/FAc Michaelis complex. The bound FAc reveals the key enzyme−substrate interactions (dashed lines with distances in Å). (C) The His280Asn/FAc covalent intermediate. The location where the displaced fluoride ion may be transiently bound is shown. (D) The WT/glycolate (GOA) product complex. (E) The initial S_N2 attack is deduced from the superposition of FAc as found in the Michaelis complex onto the structure of the covalent intermediate. The arrow shows the displacement of the substrate's C2 atom as this occurs. The location where the expelled fluoride ion may be transiently bound is indicated. (F) The same structural comparison viewed down the line of the atoms involved in the nucleophilic attack (i.e., from fluorine to the substrate's C2 to Asp110's Oδ2). The halide-stabilizing residues (His155, Trp156, and Tyr219) form a "claw" reaching for the leaving fluoride. Phe40 and Trp185 are also sufficiently close to participate in catalysis. The "flapping" motion of the indole side chain of Trp185 is indicated by the curved arrow. (G) Subsequent hydrolysis of the covalent intermediate is inferred from the superposition of the glycolyl-Asp110 residue as found in the covalent intermediate onto the enzyme−product complex. This step employs the catalytic water activated by His280. The arrow indicates how the product glycolate (GOA) detaches from its former covalent bonding partner. The omit $F_o - F_c$ electron density maps are contoured at 3σ.

dx.doi.org/10.1021/ja200277d |*J. Am. Chem. Soc.* 2011, 133, 7461–7468

Table 2. Steady-State Kinetics of RPA1163 and Mutants[a]

	fluoroacetate				chloroacetate			
enzyme	k_{cat} (min^{-1})	%	K_m (mM)	k_{cat}/K_m (s^{-1} M^{-1})	k_{cat} (min^{-1})	%	K_m (mM)	k_{cat}/K_m (s^{-1} M^{-1})
WT[b]	6.7 ± 0.6	100	3.3 ± 0.2	33	1.38 ± 0.07	21	1.6 ± 0.5	14
Phe40Ala	0.21 ± 0.04	3.1	4.4 ± 0.8	0.79	0.029 ± 0.009	0.44	1.5 ± 0.4	0.32
His155Asn	0.70 ± 0.06	11	2.9 ± 0.2	4.1	5.3 ± 0.5	79	2.0 ± 0.3	45
Trp156His	0.11 ± 0.01	1.7	8 ± 3	0.22	0.10 ± 0.02	1.5	6 ± 1	0.27
Trp185Phe	0.59 ± 0.04	8.8	3.3 ± 0.6	2.9	0.32 ± 0.04	4.7	1.0 ± 0.3	5.0
Tyr219Phe	0.035 ± 0.009	0.53	1.7 ± 0.2	0.34	0.42 ± 0.04	6.3	1.00 ± 0.07	7.0

[a] The parameters were determined from at least triplicate measurements, and the standard deviations are shown. The % activity normalizes all k_{cat} to FAc hydrolysis by WT. [b] Data from ref 30.

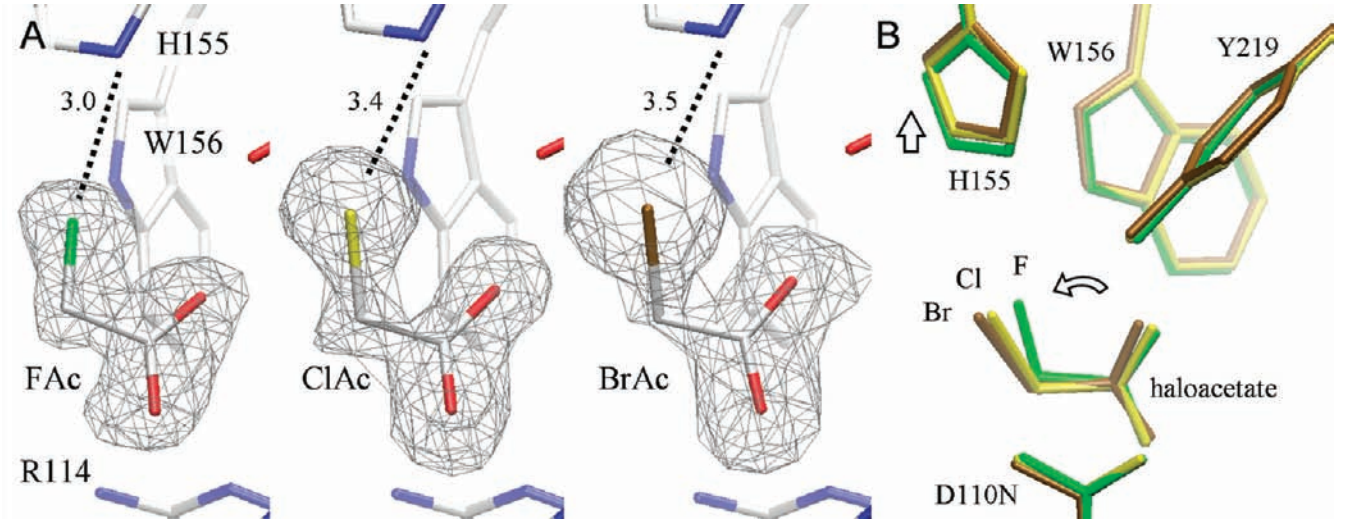

Figure 5. RPA1163 Asp110Asn mutant in complex with fluoro-, chloro-, and bromoacetate. (A) Binding of FAc, BrAc, and ClAc in the active site of the Asp110Asn mutant. FAc is bound at full occupancy, but only ~75% saturation for ClAc and BrAc is observed. The residual electron densities on O2 of ClAc and BrAc are both modeled as a chloride ion at ~25% occupancy (Supporting Information, Figure S3). The omit $F_o - F_c$ electron density maps are contoured at 4.5 (FAc), 3.0 (ClAc), and 2.8 (BrAc) σ. (B) Superposition of the FAc, ClAc, and BrAc complexes (in green, yellow, and brown, respectively) using all Cα atoms of the protein subunits. Only His155 is displaced, albeit minimally, by the increasingly larger halide of the substrate (vertical arrow). The binding of the larger halogen atom forces a slight tilt to the entire haloacetate substrate, thereby keeping the halogen atom farther out of the active site (curved arrow).

which apparently reveals a "flapping" motion in which the indole side chain sweeps by the cavity of the halide pocket (Supporting Information, Figure S2B,C).

Trp185 appears most dynamic in the absence of substrate, as suggested by its poorly defined electron density and its multiple conformations (Figure 6). In one major conformation, Trp185's indole ring is swung into the active site cavity, analogous to a door opening inward (see also Figure 3B). In the other major conformation, the side chain blocks access to the active site channel. Trp185 adopts the former (tucked in/open) conformation in both the Michaelis complex and the covalent intermediate but an intermediary conformation in the WT/glycolate product complex (Figure 6). We speculate that Trp185 is initially tucked in during substrate binding to help occlude water molecules near the halide pocket from the otherwise larger active site cavity. If Trp185 were mobile during the catalytic cycle, its side chain could come as close as ~2.8 Å (Cη2--F) to the fluoride ion, suggesting a potential interaction. The nonidentical k_{cat} values of FAc and ClAc hydrolysis in the Trp185Phe mutant (Table 2) also seem to indicate Trp185's connection to the halide. However, whether this imparts substrate recognition, C−X bond cleavage, or halide dissociation remains to be determined.

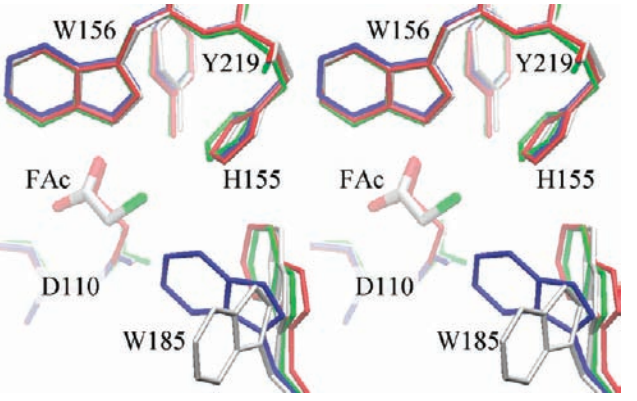

Figure 6. Stereoview comparison of different Trp185 conformations in various defluorinase complexes. The active site residues from WT/apo (gray), Asp110Asn/FAc Michaelis complex (green), His280Asn/FAc covalent intermediate (red), and WT/GOA product complex (blue) are shown.

Additional marked structural variations and disorder are found in a second loop formed by residues 251−259, which covers part of the active site entrance (Supporting Information, Figure S2A). We speculate that this segment may regulate substrate entry and product dissociation.

CONCLUSION

S_N2 reactions, despite being a staple in organic chemistry, are rather few in the biological realm; many are based on the widely used group-transfer reactions involving *S*-adenosyl methionine or its derivatives.[32] Nevertheless, it is a reaction strategy employed by many dehalogenases, including haloalkane dehalogenases, fluoroacetate dehalogenases, L-2-haloacid dehalogenases, D- and DL-2-haloacid dehalogenases, haloalcohol dehalogenases, and dichloromethane dehalogenases. However, only the fluoroacetate dehalogenases and a few novel L-2-haloacid dehalogenases have acquired defluorination activity.[30] It was proposed that FAcDs can defluorinate because they supply three electrostatic contacts or hydrogen bonds to activate the C−F bond.[28] This contrasts with the non-defluorinating dehalogenases, which appear to use fewer such contacts for breaking the weaker C−X bonds.[26,33−37] However, our results suggest that defluorination further requires the close and most precise placement of the binding residues in order to effectively stabilize the small fluoride ion. Interestingly, nucleophilic substitution is also employed by some halogenases to catalyze the reverse reaction,[32] but only the *Streptomyces cattleya* enzyme can form the C−F bond.[38] The halide pocket of this fluorinase is similar to that of FAcDs in that it is small and forms three contacts with the fluoride.[39−41] This appears to be a common strategy for directing fluorine biochemistry in addition to establishing fluoride selectivity.

Nature has also evolved other enzymes which can break strong chemical bonds such as N≡N, C≡N, C≡C, C═C, or C═O. However, these enzymes are mostly oxidoreductases (e.g., nitrogenases or CO dehydrogenases) that require high energy input in the form of ATP and/or low-potential electrons. A few organofluorines appear to be defluorinated anaerobically and may act as electron acceptors for certain reductive dehalogenases, but the underlying catalytic mechanism is still unknown, and it is unclear whether reductive dehalogenases can cleave the C−F bond.[12,13] In contrast, RPA1163 and other related defluorinases are able to break this strong bond without the need for external energy input.

The high-resolution crystal structures of RPA1163 provide a detailed molecular view of biocatalytic defluorination, which requires three closely and precisely positioned polar contacts/hydrogen bonds to activate and stabilize the small fluorine atom, and protein motions with a potential functional relevance are identified. These results lay the foundations for future biotechnological developments, with a view toward viable sustainable management and disposal practices for the valuable but persistent fluorinated organic products.

MATERIALS AND METHODS

Materials. The Ni-NTA resin and QIAprep spin miniprep kit were purchased from Qiagen (Mississauga, Canada) and the QuikChange site-directed mutagenesis kit from Stratagene (La Jolla, CA). Lysogeny broth and terrific broth pellets were obtained from EMD Chemicals (Gibbstown, NJ); agar, ampicillin, kanamycin, glycerol, HEPES, IPTG, and Tris from BioShop (Burlington, Canada); sodium fluoroacetate, chloroacetic acid, and bromoacetic acid from Sigma-Aldrich (St. Louis, MO); and bromothymol blue from Fisher Scientific (Ottawa, Canada). The oligonucleotides were synthesized by Integrated DNA Technologies (Coralville, IA). Paratone N was purchased from Hampton Research (Aliso Viejo, CA). All purchased chemicals were of the highest grades commercially available.

Protein Purification. Protein purification was performed as described.[30] In brief, the protein was purified from the *E. coli* cell-free extract by Ni-affinity chromatography, followed by cleavage of the His_6-tag using TEV protease and a second round of Ni-affinity chromatography. The protein was further purified by size exclusion chromatography in 150 mM NaCl and 50 mM Tris-H_2SO_4 pH 8.5, buffer-exchanged into 50 mM Tris-H_2SO_4 pH 8.5, and finally flash-frozen in liquid nitrogen. Protein concentrations were determined from their absorbance at 280 nm using extinction coefficients derived by ProtPARAM.[42]

Site-Directed Mutagenesis. Site-directed mutagenesis was performed using QuikChange according to the manufacturer's instructions.

Crystallization. Crystals in space group $P2_12_12_1$ were produced by hanging drop, in 16−20% PEG3350, 200 mM NH_4Cl and 100 mM sodium cacodylate pH 6.5, using as seed WT parent crystals grown with the supplementation of 4% sucrose. $P2_1$ crystals were grown in 15−24% PEG3350, 100−200 mM $CaCl_2$ and 100 mM Tris-HCl pH 7.5. All enzyme-ligand complexes were produced by soaking crystals in mother liquor supplemented with the respective ligand (Supporting Information, Table S1).

Structure Determination and Manipulation. Diffraction data were collected at cryogenic temperature, using paratone N as cryoprotectant. Data were reduced with XDS[43] and the structures refined iteratively with the help of Refmac5 in the CCP4i crystallographic software package and Coot.[44−46] Anisotropic *B* factors were refined for data sets with resolutions better than 1.2 Å. The phases were initially solved by molecular replacement with Phaser[47] using a homology model built by Phyre[48] from the *Burkholderia* FAcD structure (PDB code: 1Y37). The PRODRG web server was used for generating the coordinates and restraint parameters of ligands and modified amino acid residues.[49] The secondary structure matching algorithm SSM aligning all Cα atoms was employed in all structural comparisons unless specified otherwise.[50] Graphical representations of protein structures were generated in VMD.[51] The atomic coordinates and structure factors have been deposited into the RCSB Protein Data Bank under PDB codes listed in Table 1 and Supporting Information, Table S1.

Isothermal Microcalorimetry. Steady-state kinetics were measured by microcalorimetry in at least triplicate in 100 mM Tris-H_2SO_4 pH 8.5 at 30 °C using the VP-ITC microcalorimeter (MicroCal, LLC, Northampton, MA). The principles and procedures have been described.[30,52] The nature of the reaction (i.e., product inhibition and irreversibility) was first characterized by consecutive single-injection experiments. The apparent reaction enthalpy (ΔH_{app}) for each substrate was calculated directly from the peak areas without consideration of equilibrium because the reaction was shown to be virtually irreversible.[30] Multiple-injection experiments were performed because of product inhibition. Substrate was injected as 6 × 3 μL, 6 × 10 μL, and 6 × 32 μL at approximately 4 min intervals, and the final concentrations accumulated approximately from $K_m/10$ to $10\times K_m$ whenever achievable. The k_{cat} and K_m were extracted by nonlinear regression using the software package Origin (MicroCal, LLC).

Colorimetric Dehalogenation Assays. Dehalogenation activity was monitored through the proton released in a weakly buffered system, which is coupled to the color change of a pH indicator for detection.[53] The reaction was performed in a volume of 1 mL. The final concentrations of the assay components were 10 mM sodium haloacetate, 1 mM Tris-H_2SO_4 pH 8.5, 20 μg/mL bromothymol blue, and 150 μg/mL WT RPA1163. The absorbance at 616 nm was recorded. The background

drift of A_{616} was measured for 2 min before the addition of enzyme. The enzymatic reaction was then monitored for 3 min, and the net change in slope was used for calculating the reaction rate. The final values are averaged from triplicate runs.

■ ASSOCIATED CONTENT

Supporting Information. Table of crystallographic statistics, sequence alignment of FAcDs, structural variations and ligand binding of RPA1163, structural influence of mutations and crystal packing, pH-based assays of haloacetates, and thermodynamics of hydrolytic defluorination. This material is available free of charge via the Internet at http://pubs.acs.org.

■ AUTHOR INFORMATION

Corresponding Author
pai@hera.med.utoronto.ca

■ ACKNOWLEDGMENT

We thank Aled M. Edwards for a critical review of the manuscript and Aiping Dong, Yan Liu, Xiaohui Xu, and Hong Zheng for their technical assistance. We are also grateful to the beamline staff at BioCARS and the Structural Biology Center (SBC) at Argonne National Laboratory for their help during data collection. The results shown in this report are derived from work performed at Argonne National Laboratory, BioCARS, and SBC at the Advanced Photon Source. Argonne is operated by the University of Chicago Argonne, LLC, for the U.S. Department of Energy, Office of Biological and Environmental Research, under contract DE-AC02-06CH11357. Use of the BioCARS Sector 14 was supported by the National Institutes of Health, National Center for Research Resources, under grant No. RR007707. The research was supported by the Natural Sciences and Engineering Research Council of Canada through a graduate scholarship (P.W.Y.C.) and operating grants (E.A.E. and E.F.P.) and by the Canada Research Chairs Program (E.F.P.).

■ REFERENCES

(1) Goldman, P. *Science* **1969**, *164*, 1123–1130.
(2) Lemal, D. M. *J. Org. Chem.* **2004**, *69*, 1–11.
(3) O'Hagan, D. *Chem. Soc. Rev.* **2008**, *37*, 308–319.
(4) Douvris, C.; Ozerov, O. V. *Science* **2008**, *321*, 1188–1190.
(5) Smart, B. E. *J. Fluor. Chem.* **2001**, *109*, 3–11.
(6) Ritter, S. K. *Chem. Eng. News* **2010**, *88*, 12–17.
(7) Key, B. D.; Howell, R. D.; Criddle, C. S. *Environ. Sci. Technol.* **1997**, *31*, 2445–2454.
(8) Muller, K.; Faeh, C.; Diederich, F. *Science* **2007**, *317*, 1881–1886.
(9) Calafat, A. M.; Wong, L. Y.; Kuklenyik, Z.; Reidy, J. A.; Needham, L. L. *Environ. Health Perspect.* **2007**, *115*, 1596–1602.
(10) Houde, M.; Martin, J. W.; Letcher, R. J.; Solomon, K. R.; Muir, D. C. *Environ. Sci. Technol.* **2006**, *40*, 3463–3473.
(11) Shine, K. P.; Sturges, W. T. *Science* **2007**, *315*, 1804–1805.
(12) Natarajan, R.; Azerad, R.; Badet, B.; Copin, E. *J. Fluor. Chem.* **2005**, *126*, 424–435.
(13) Murphy, C. D. *Biotechnol. Lett.* **2010**, *32*, 351–359.
(14) Au, K. G.; Walsh, C. T. *Bioorg Chem* **1984**, *12*, 197–205.
(15) Kurihara, T.; Esaki, N. *Chem. Rec.* **2008**, *8*, 67–74.
(16) Kurihara, T.; Yamauchi, T.; Ichiyama, S.; Takahata, H.; Esaki, N. *J. Mol. Catal. B: Enzymol.* **2003**, *23*, 347–355.
(17) Liu, J. Q.; Kurihara, T.; Ichiyama, S.; Miyagi, M.; Tsunasawa, S.; Kawasaki, H.; Soda, K.; Esaki, N. *J. Biol. Chem.* **1998**, *273*, 30897–30902.
(18) *Hazardous Substances Data Bank*; U.S. National Library of Medicine: Bethesda, MD.
(19) O'Hagan, D.; B. Harper, D. *J. Fluor. Chem.* **1999**, *100*, 127–133.
(20) Murphy, C. D.; Schaffrath, C.; O'Hagan, D. *Chemosphere* **2003**, *52*, 455–461.
(21) Peters, R.; Wakelin, R. W. *Proc. R. Soc. London B: Biol. Sci.* **1953**, *140*, 497–507.
(22) Proudfoot, A. T.; Bradberry, S. M.; Vale, J. A. *Toxicol. Rev.* **2006**, *25*, 213–219.
(23) Holmquist, M. *Curr. Protein Pept. Sci.* **2000**, *1*, 209–235.
(24) Verschueren, K. H.; Seljee, F.; Rozeboom, H. J.; Kalk, K. H.; Dijkstra, B. W. *Nature* **1993**, *363*, 693–698.
(25) de Jong, R. M.; Dijkstra, B. W. *Curr. Opin. Struct. Biol.* **2003**, *13*, 722–730.
(26) Schmidberger, J. W.; Wilce, J. A.; Tsang, J. S.; Wilce, M. C. *J. Mol. Biol.* **2007**, *368*, 706–717.
(27) Jitsumori, K.; Omi, R.; Kurihara, T.; Kurata, A.; Mihara, H.; Miyahara, I.; Hirotsu, K.; Esaki, N. *J. Bacteriol.* **2009**, *191*, 2630–2637.
(28) Kamachi, T.; Nakayama, T.; Shitamichi, O.; Jitsumori, K.; Kurihara, T.; Esaki, N.; Yoshizawa, K. *Chemistry* **2009**, *15*, 7394–7403.
(29) Siegel, J. B.; Zanghellini, A.; Lovick, H. M.; Kiss, G.; Lambert, A. R.; St Clair, J. L.; Gallaher, J. L.; Hilvert, D.; Gelb, M. H.; Stoddard, B. L.; Houk, K. N.; Michael, F. E.; Baker, D. *Science* **2010**, *329*, 309–313.
(30) Chan, W. Y.; Wong, M.; Guthrie, J.; Savchenko, A. V.; Yakunin, A. F.; Pai, E. F.; Edwards, E. A. *Microb. Biotechnol.* **2010**, *3*, 107–120.
(31) Bach, R. D.; Coddens, B. A.; Wolber, G. J. *J. Org. Chem.* **1986**, *51*, 1030–1033.
(32) O'Hagan, D.; Schmidberger, J. W. *Nat. Prod. Rep.* **2010**, *27*, 900–918.
(33) Bohac, M.; Nagata, Y.; Prokop, Z.; Prokop, M.; Monincova, M.; Tsuda, M.; Koca, J.; Damborsky, J. *Biochemistry* **2002**, *41*, 14272–14280.
(34) Schmidberger, J. W.; Wilce, J. A.; Weightman, A. J.; Whisstock, J. C.; Wilce, M. C. *J. Mol. Biol.* **2008**, *378*, 284–294.
(35) Marsh, A.; Ferguson, D. M. *Proteins* **1997**, *28*, 217–226.
(36) de Jong, R. M.; Kalk, K. H.; Tang, L.; Janssen, D. B.; Dijkstra, B. W. *J. Bacteriol.* **2006**, *188*, 4051–4056.
(37) de Jong, R. M.; Tiesinga, J. J.; Rozeboom, H. J.; Kalk, K. H.; Tang, L.; Janssen, D. B.; Dijkstra, B. W. *Embo J.* **2003**, *22*, 4933–4944.
(38) Dong, C.; Huang, F.; Deng, H.; Schaffrath, C.; Spencer, J. B.; O'Hagan, D.; Naismith, J. H. *Nature* **2004**, *427*, 561–565.
(39) Zhu, X.; Robinson, D. A.; McEwan, A. R.; O'Hagan, D.; Naismith, J. H. *J. Am. Chem. Soc.* **2007**, *129*, 14597–14604.
(40) Eustaquio, A. S.; Pojer, F.; Noel, J. P.; Moore, B. S. *Nat. Chem. Biol.* **2008**, *4*, 69–74.
(41) Blasiak, L. C.; Drennan, C. L. *Acc. Chem. Res.* **2009**, *42*, 147–155.
(42) Wilkins, M. R.; Gasteiger, E.; Bairoch, A.; Sanchez, J. C.; Williams, K. L.; Appel, R. D.; Hochstrasser, D. F. *Methods Mol. Biol.* **1999**, *112*, 531–552.
(43) Kabsch, W. *J. Appl. Crystallogr.* **1993**, *26*, 795–800.
(44) Murshudov, G. N.; Vagin, A. A.; Dodson, E. J. *Acta Crystallogr. D: Biol. Crystallogr.* **1997**, *53*, 240–255.
(45) Emsley, P.; Lohkamp, B.; Scott, W. G.; Cowtan, K. *Acta Crystallogr. D: Biol. Crystallogr.* **2010**, *66*, 486–501.
(46) CCP4 *Acta Crystallogr. D: Biol. Crystallogr.* **1994**, *50*, 760–763.
(47) McCoy, A. J.; Grosse-Kunstleve, R. W.; Adams, P. D.; Winn, M. D.; Storoni, L. C.; Read, R. J. *J. Appl. Crystallogr.* **2007**, *40*, 658–674.
(48) Kelley, L. A.; Sternberg, M. J. *Nat. Protoc.* **2009**, *4*, 363–371.
(49) Schuttelkopf, A. W.; van Aalten, D. M. *Acta Crystallogr. D: Biol. Crystallogr.* **2004**, *60*, 1355–1363.
(50) Krissinel, E.; Henrick, K. *Acta Crystallogr. D: Biol. Crystallogr.* **2004**, *60*, 2256–2268.
(51) Humphrey, W.; Dalke, A.; Schulten, K. *J. Mol. Graph.* **1996**, *14*, 33–38.
(52) Todd, M. J.; Gomez, J. *Anal. Biochem.* **2001**, *296*, 179–187.
(53) Holloway, P.; Trevors, J. T.; Lee, H. *J. Microbiol. Methods* **1998**, *32*, 31–36.